RANS COMPUTATIONS OF RECIRCULATING FLOWS AT LOW REYNOLDS NUMBERS

Gorazd Medic
Flow Physics & Computation Division,
Stanford University,
Stanford, CA 94305-3030, USA
gmedic@stanford.edu

Georgi Kalitzin
Flow Physics & Computation Division,
Stanford University,
Stanford, CA 94305-3030, USA
kalitzin@stanford.edu

ABSTRACT

The behavior of four RANS turbulence models (v^2-f, Spalart-Allmaras, k-ω and its low-Re counterpart) is investigated for recirculating flows at low Reynolds numbers. It is shown that significant difficulties are caused by the transitional nature of the flow. The low-Re correction for the k-ω model fails to improve the results.

Detailed look at the flat plate solutions at various Reynolds numbers show that only for the high-Re k-ω model the turbulence production P_k^+ collapses on a single solution for all investigated Reynolds numbers.

INTRODUCTION

The ability of RANS turbulence models to capture pressure driven separation and reattachment at low Reynolds numbers is studied in this paper. The low-Re modifications of turbulence models are often designed to capture transition to turbulence for flow over a flat plate (for an example see the discussion in Wilcox, 1993). However, recent computations with low-Re models for recirculating flows in arterial stenoses (see Medic, 2005) indicate that these low-Re modifications fail to predict flows that transition to turbulence under a different scenario. Pulsating blood flow in arteries is at relatively low Reynolds number, but it has been shown that various artery constrictions lead to large separation and effectively to turbulent flow. Successful modeling of these low Reynolds turbulent flows is of great importance in biomechanical engineering and design of interventional devices such as stents. Therefore a more thorough analysis of RANS turbulence models used for computations at low Reynolds numbers is warranted.

RECIRCULATING FLOW AT LOW-REYNOLDS NUMBERS

A very simple and easily reproducible test problem is analyzed here: the boundary layer over a flat plate with an imposed streamwise pressure gradient. This flow was computed using direct numerical simulation (DNS) by Na and Moin (1996) and an extensive database is available. The pressure gradient is modulated by suction and blowing applied at a given distance from the plate (see Figure 1). The inflow profile is obtained from Spalart's DNS (Spalart, 1988) for Reynolds number $Re_\theta = 300$. The dimensions of the computational domain are: $350\delta^*_{in} \times 64\delta^*_{in}$, where δ^*_{in} is the displacement thickness for the inflow profile. The vertical velocity component at the upper boundary is defined as:

$$v(x) = A(x_0 - x)e^{-b(x_0-x)^2} \tag{1}$$

with $A = 0.019u_\infty/\delta^*_{in}$, $b = 2.3110^{-4}/{\delta^*_{in}}^2$ and $x_0 = 221.4\delta^*_{in}$.

This test case is attractive for detailed analysis of the performance of RANS turbulence models since it eliminates the uncertainty related to the effects of curvature and the quality of computational grid usually associated with the recirculating flows (for example, for the flow over a bump or the flow through an arterial stenosis).

A Cartesian incompressible RANS flow solver (Kalitzin and Iaccarino, 2003) is used and results obtained with four turbulence models are presented: v^2-f (the modified version with N=6, Lien and Durbin, 1996), Spalart-Allmaras (Spalart and Allmaras, 1994), k-ω and its low-Re counterpart (Wilcox, 1993). The low-Reynolds number corrections for the k-ω model (Wilcox, 1993) are:

$$\nu_T = \alpha^* \frac{k}{\omega},\ \alpha^* = \frac{\alpha_0^* + Re_T/R_k}{1 + Re_T/R_k}$$

$$\alpha = \frac{1}{\alpha^*}\frac{5}{9}\frac{\alpha_0 + Re_T/R_\omega}{1 + Re_T/R_\omega},\ \beta^* = \frac{9}{100}\frac{5/18 + (Re_T/R_\beta)^4}{1 + (Re_T/R_\beta)^4} \tag{2}$$

$$R_\beta = 8,\ R_k = 6,\ R_\omega = 2.7,\ Re_T = k/(\nu\omega)$$

The inflow profile for the turbulent kinetic energy is computed from Spalart's DNS turbulence intensities $k = (u^2_{rms} + v^2_{rms} + w^2_{rms})/2$, the profile for $\overline{v^2}$ is set to v^2_{rms} and the eddy-viscosity is computed from the Reynolds stress $\nu_t = - < uv > /(dU/dy)$. While ω follows explicitly, ε and $\tilde{\nu}$ are obtained iteratively from the eddy-viscosity definition. df/dn is set to zero.

Streamlines and contours of eddy-viscosity are presented in Figure 2. The skin friction and pressure coefficients are compared with DNS data in Figure 3. The results for skin friction

show that all four turbulence models predict separation and that the reattachment location, largely affected by the blowing on the upper boundary, agrees well with the DNS. However, the location of the separation point is predicted too early and the skin friction is underpredicted upstream of the recirculation region. Most strikingly, the pressure is underpredicted in the recirculation region for the low-Re k-ω computation.

Comparison of velocity and turbulent kinetic energy profiles with DNS data is presented in Figures 4 and 5. The velocity profiles upstream of the recirculation region ($x/\delta^*_{in} = 120$) agree well with the DNS for all four models. At $x/\delta^*_{in} = 220$, the low-Re k-ω model velocity profile differs most from the DNS. In the recovery region, at $x/\delta^*_{in} = 320$, the velocity profiles are poorly predicted with all four models. The plots of turbulent kinetic energy reveal that the most significant differences are observed in the recirculation region at $x/\delta^*_{in} = 220$ where all the models overpredict the level of k. As designed, the low-Re corrections improve the overall turbulent kinetic energy predictions for the k-ω model.

The differences between RANS computations and DNS in the region upstream of the recirculation can be explained by the transitional nature of the inflow at $Re_\theta = 300$, as discussed in detail in Spalart (1988). Computations of flow over a flat plate at this Reynolds number presented in the following section illustrate the shortcomings of turbulence models investigated here.

FLOW OVER A FLAT PLATE

Flow over a flat plate at zero pressure gradient is investigated for various Reynolds numbers. Profiles of U^+, k^+, P_k^+ and $< uv >^+$ are presented in Figures 6-8. The figures also include the DNS data for $Re_\theta = 300$ from Spalart (1988). Clearly, for high Reynolds numbers the universal behavior of U^+ and $< uv >^+$ is well predicted by all models. However, for $Re_\theta = 300$, all models except the high-Re k-ω model show large discrepancies with the DNS data.

For this Reynolds number the flow is transitional and depends on the turbulence levels at the inflow. Low turbulence values are specified to retain a laminar character of the inflow. The specified turbulence quantities correspond to a turbulence intensity of $Tu = 0.01$ and an eddy-viscosity ratio of $\nu_t/\nu = 0.01$. If higher turbulence levels are used at the inflow, transition can be triggered earlier, significantly improving the low-Re k-ω model. Nevertheless, the plotted results present clearly the difficulties RANS turbulence models have in predicting flow at this low Reynolds number.

The low-Re corrections for k-ω model improve the prediction of the universal profile for k^+. As designed, these modifications force the quadratic near-wall behavior of k^+ and lead to the typical peak of k^+ at $y^+ \approx 10$. However, at $Re_\theta = 300$ the k^+ profiles start to depart from the universal behavior observed for the higher Reynolds numbers for all models considered. It is remarkable, that only for the high-Re k-ω model the turbulence production P_k^+ collapses on a single solution for all Reynolds numbers.

As observed by Spalart (1988), for $Re_\theta = 300$ the Reynolds stress $- < uv >^+$ does not approach unity in the logarithmic layer, indeed it decreases with $y^+ > 30$. This is captured properly only by the high-Re k-ω and the Spalart-Allmaras models.

CONCLUSIONS

The computations for the recirculating flow at low-Re numbers demonstrate the difficulty of capturing separation and transitional effects with RANS turbulence models. The low-Re corrections for the k-ω model improve k predictions, but velocity and pressure predictions in the recirculation region deteriorate.

Detailed look at the flat plate solutions at various Reynolds numbers show that only for the high-Re k-ω model the turbulence production P_k^+ collapses on a single solution for all Reynolds numbers. In addition, this model also predicts the correct velocity profile at $Re_\theta = 300$ despite the incorrect prediction for k^+.

REFERENCES

Lien, F.S., and Durbin, P.A., 1996, "Non-linear $k - \varepsilon - \overline{v^2}$ Modelling with Application to High Lift", *Proc. of the Summer Program 1996*, Stanford University, CA.

Kalitzin, G., and Iaccarino, G., 2003, "Toward Immersed Boundary Simulation of High Reynolds Number Flows", *CTR Annual Research Briefs*, pp. 369-378.

Medic, G., 2005, "RANS Computations of Artery Flows", *Computational Fluid and Solid Mechanics 2005*, pp. 761-765.

Na, Y., and Moin, P., 1996, "Direct Numerical Simulation of Turbulent Boundary Layers with Adverse Pressure Gradient and Separation", Ph.D. Thesis, Mech. Eng. Dept., Stanford University, CA.

Spalart, P. R., and Allmaras, S. R., 1994, "A One-Equation Turbulence Model for Aerodynamic Flows", *La Recherche Aerospatiale*, Vol. 1, pp. 1-23.

Spalart, P. R., 1988, "Direct Simulation of a Turbulent Boundary Layer up to $R_\theta = 1410$", *J. Fluid Mechanics*, Vol. 187, pp. 61-98.

Wilcox, D. C., 1993, "Turbulence Modeling for CFD", DCW Industries, Inc., La Canada, CA.

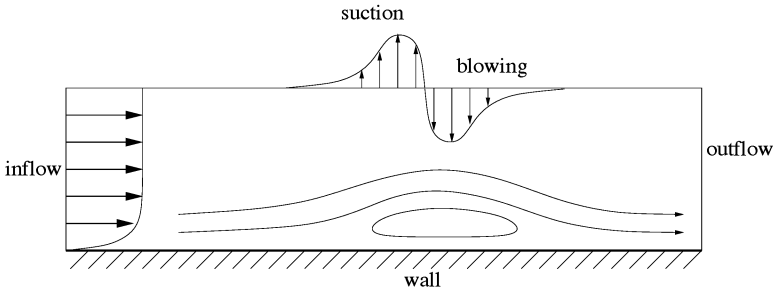

Figure 1: Flat plate with separation induced via suction and blowing at the upper boundary.

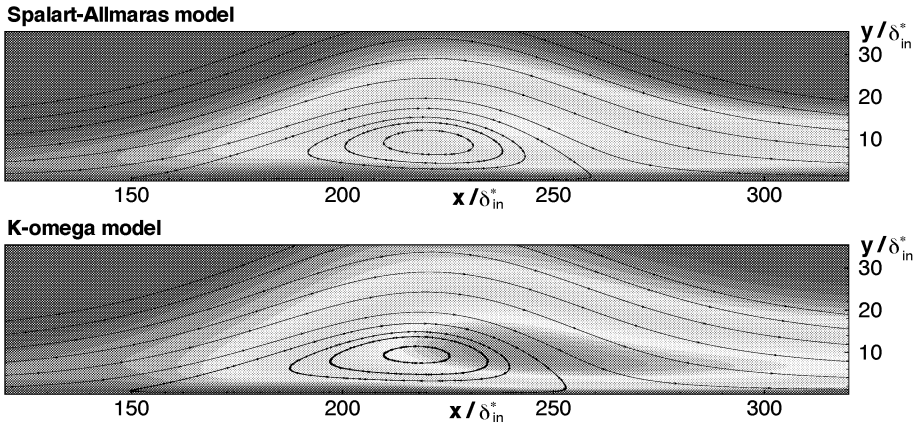

Figure 2: Streamlines and contours of eddy-viscosity for Spalart-Allmaras and k-ω models.

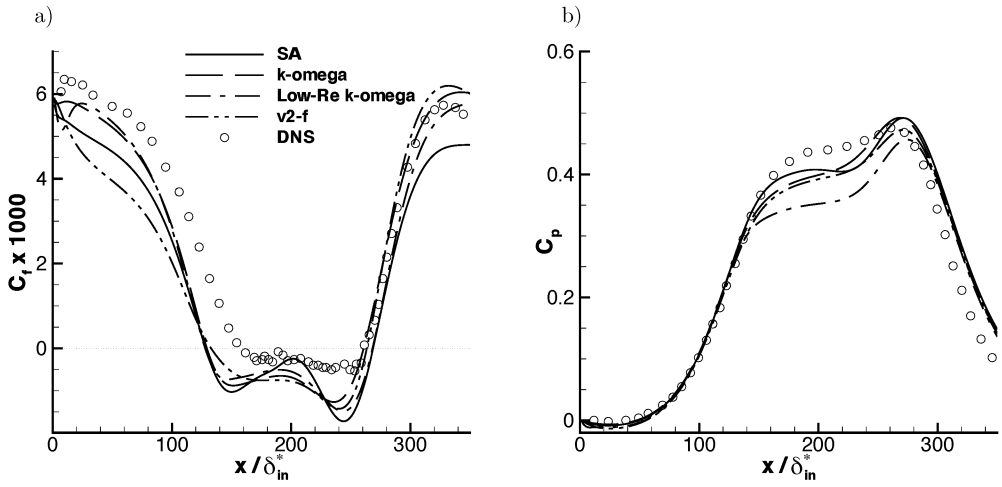

Figure 3: Skin friction (a) and pressure coefficient (b)

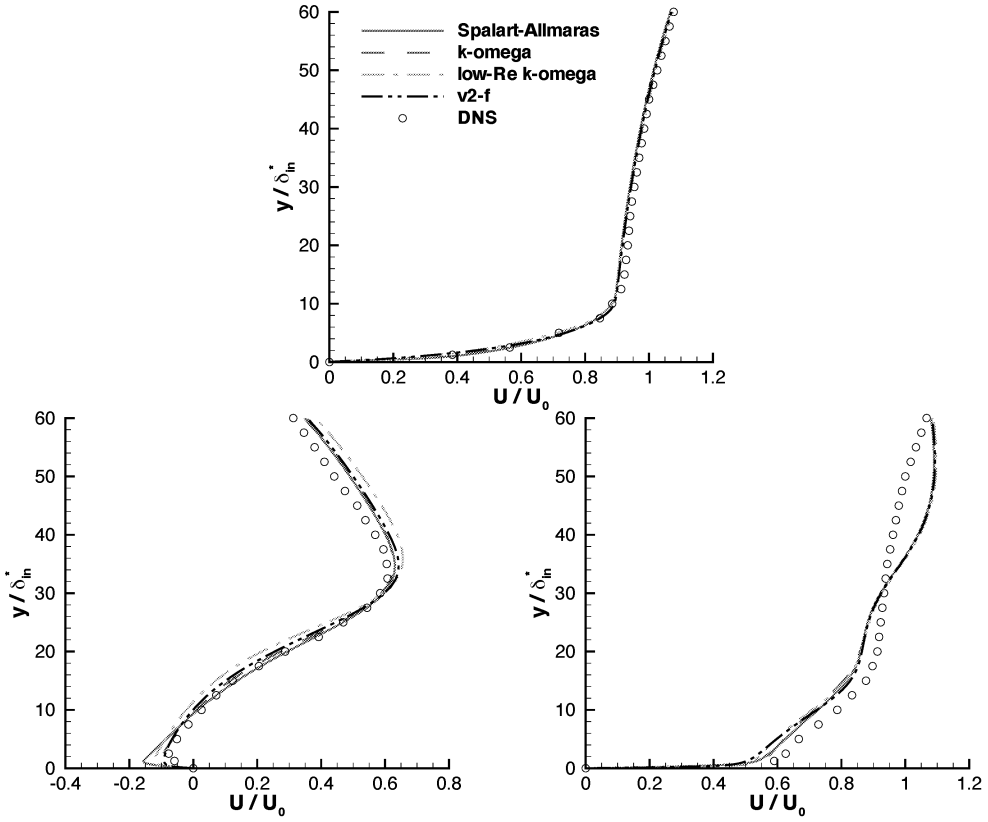

Figure 4: Streamwise velocity U at $x/\delta^*_{in} = 120$, 220 and 320

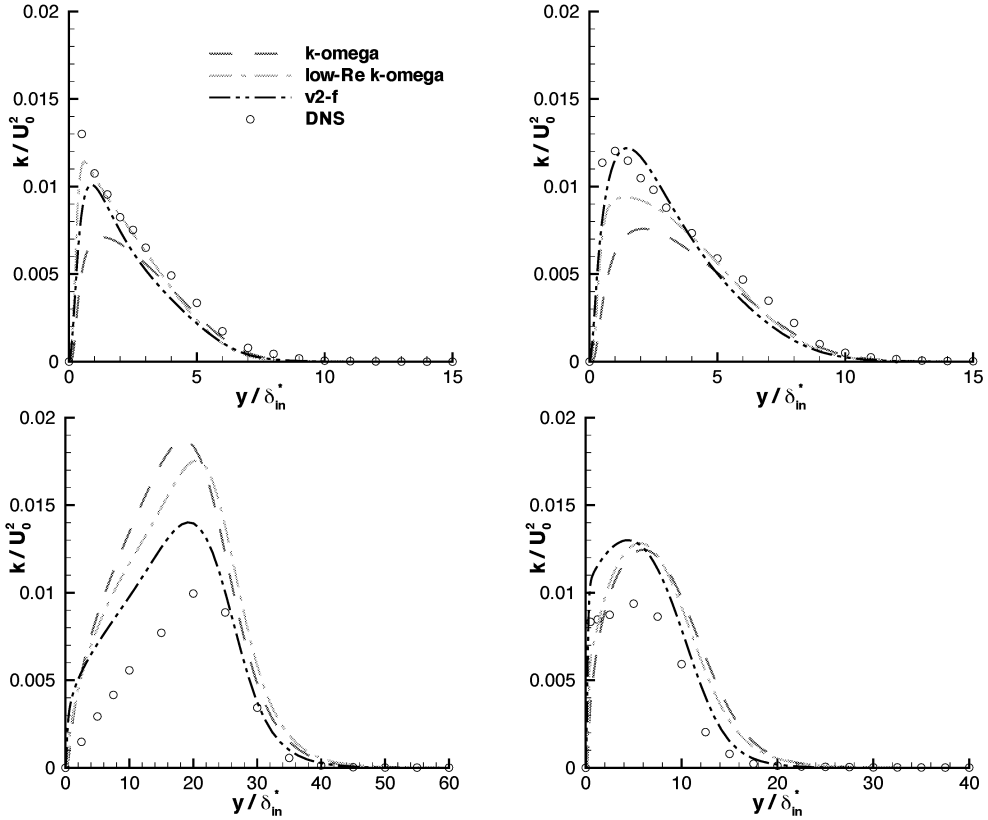

Figure 5: Turbulent kinetic energy k at $x/\delta^*_{in} = 80$, 120, 220 and 320

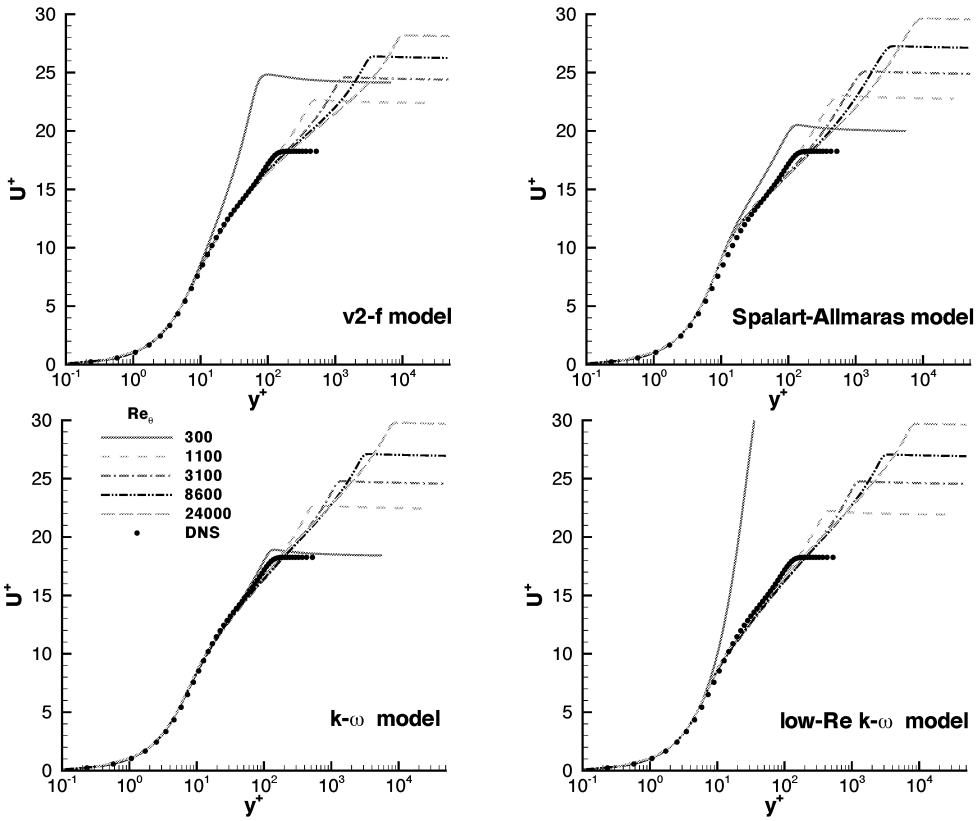

Figure 6: Velocity U^+ for various Re_θ

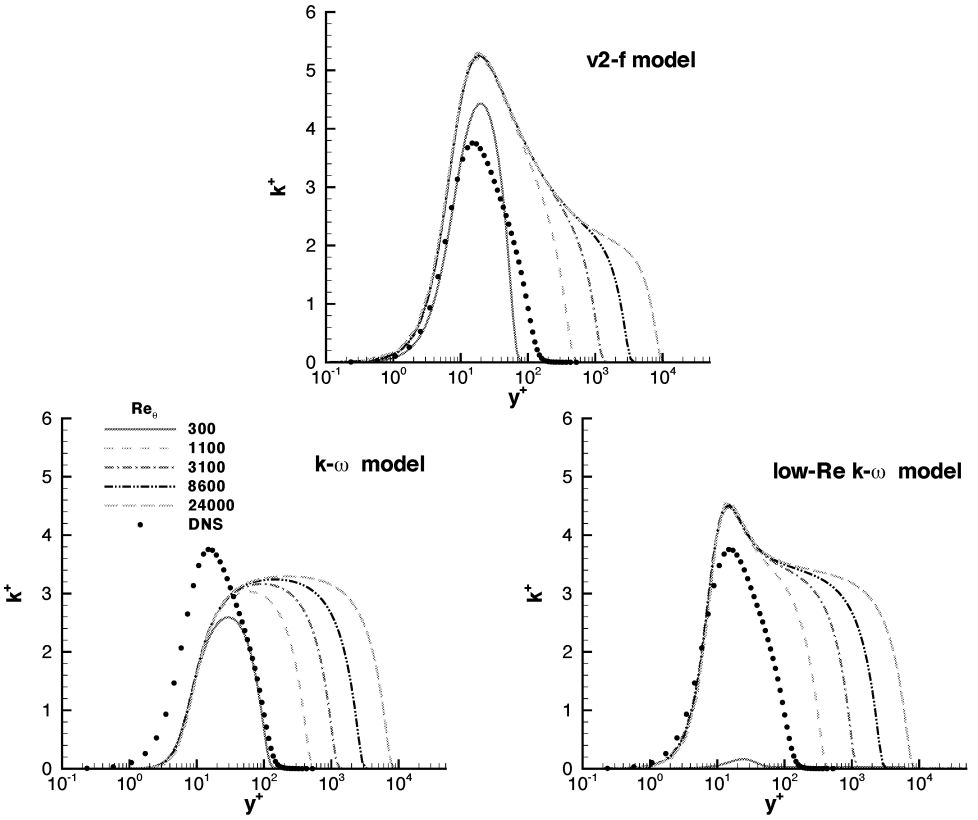

Figure 7: Turbulent kinetic energy k^+ for various Re_θ

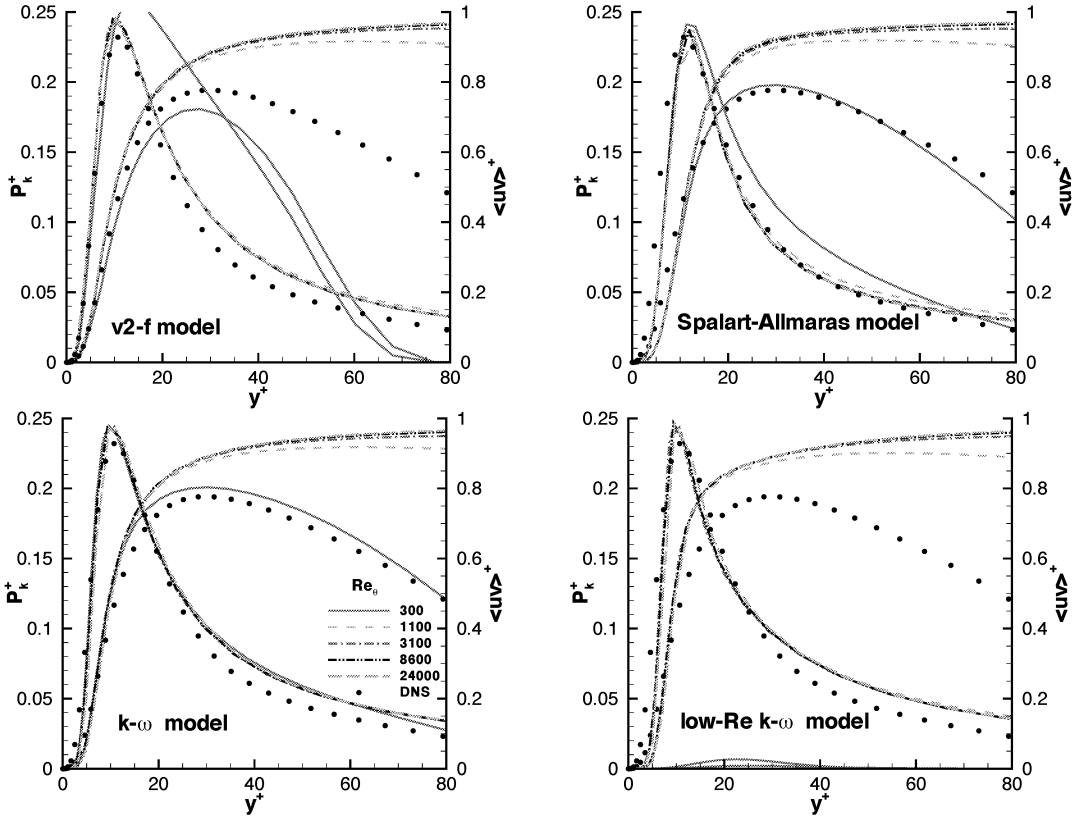

Figure 8: P_k^+ and $< uv >^+$ for various Re_θ